Connected and Disconnected Contributions to Nucleon Form Factors and Parton Distributions

Saraswati Pandey

University of Virginia

Based on: arXiv:2512.20853 **(under review PRL)** **and** arXiv:2511.03065 **(accepted in EPJC)**

Zaki Panjsheeri, Saraswati Pandey **and** Simonetta Liuti

Light Cone 2026:Applications at EIC era (LC 2026)

Stony Brook University

Center for Frontiers in Nuclear Science

STONY BROOK UNIVERSITY + BROOKHAVEN NATIONAL LABORATORY

Outline

- Motivation
- Introduction
  - Generalized Parton Distributions
- Disconnected Distributions from Lattice QCD
- Possible Approach (UVA2)
  - Calculations
- Results
- Conclusions
- Future Motivation

Motivation

- ❑ To have unified QCD picture of the spatial 3D structure of proton
  - ❑ Quantification of light flavors to the nucleon form factors
  - ❑ Contribution of anti-quarks
  - ❑ Role of gluons in there

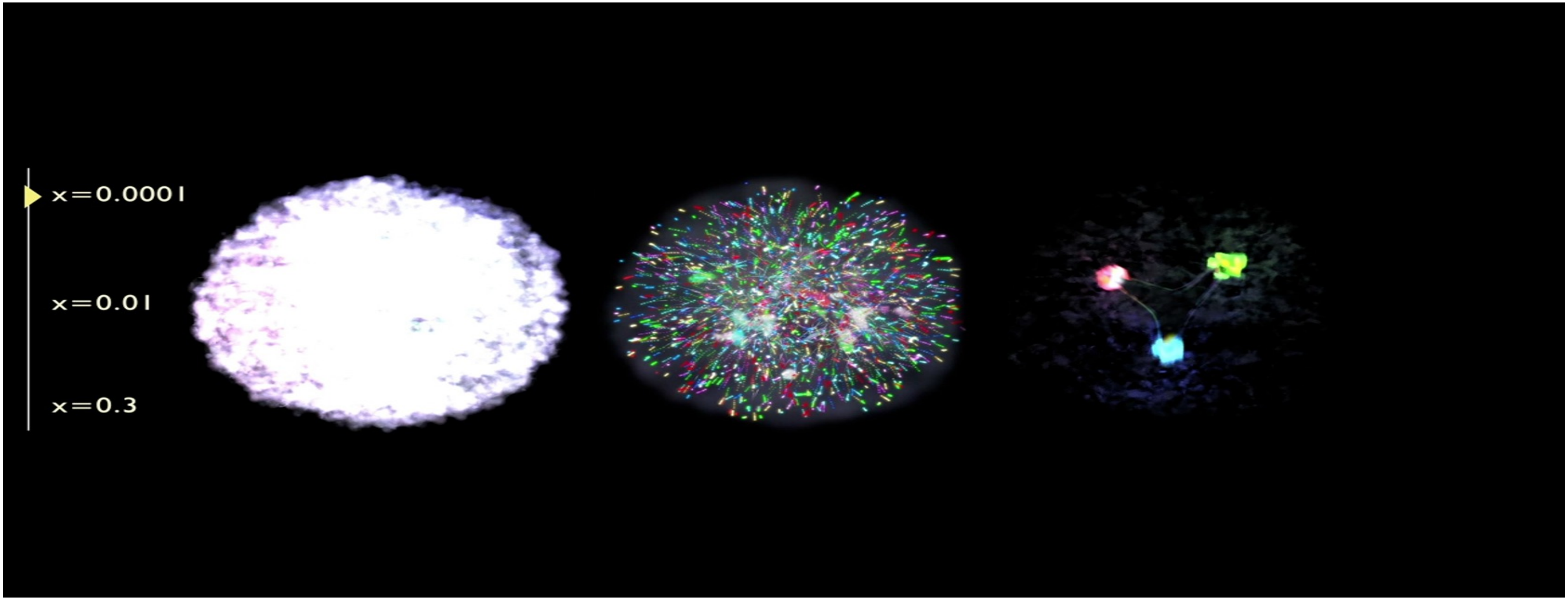

visualizing proton
presented by the MIT Center for Art, Science & Technology, Jefferson Lab, and US Department of Energy's Office of Science.

Introduction

- Current Understanding of internal structure of proton
  - Flavor separation and dominance of nucleon form factors
  - Sea quark contribution
  - Heavy flavor asymmetry
  - Gluon contributions (baryon junctions)

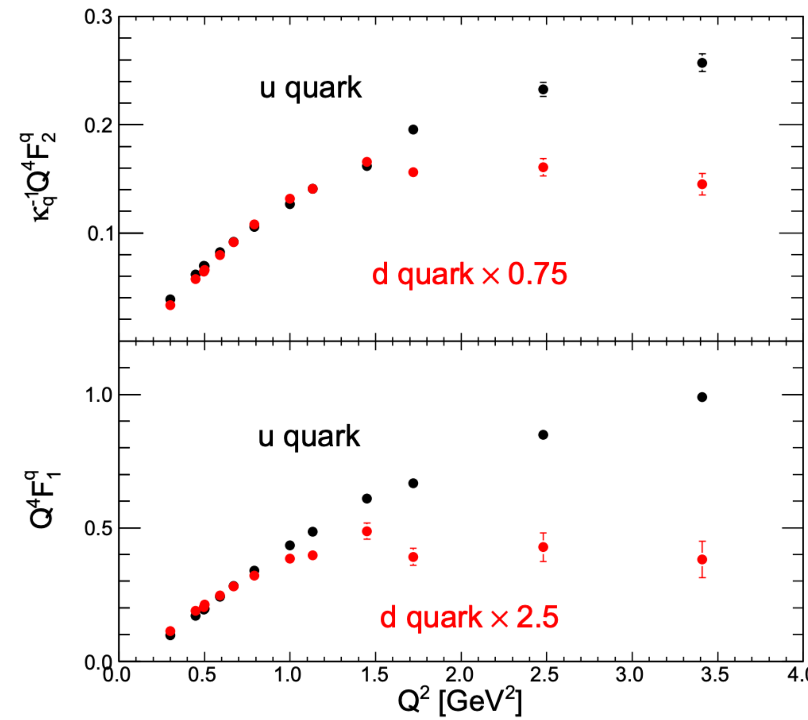

G. D. Cates et al.
Phys. Rev. Lett. 106, 252003 (2011)

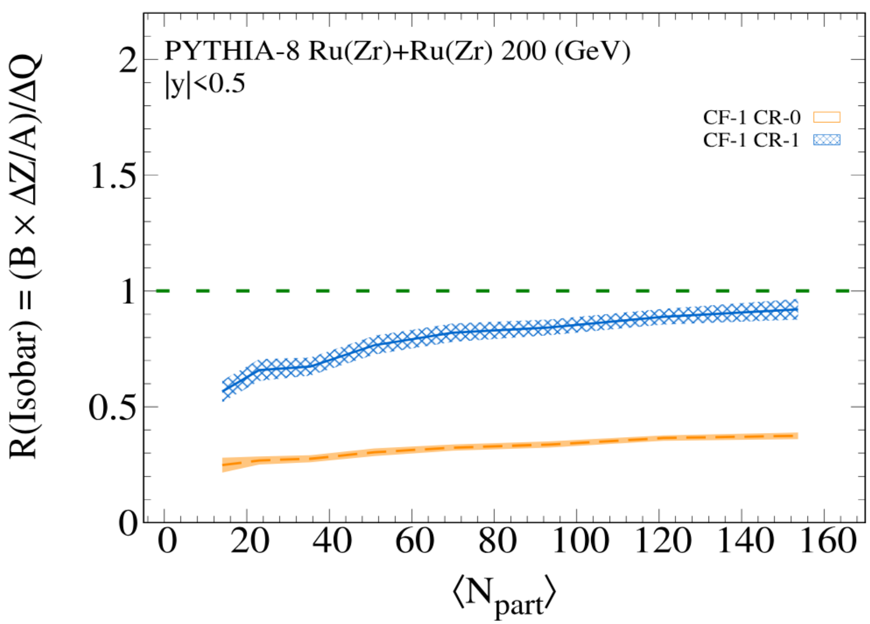

N. Magdy, et al.
Phys. Rev. C 112, 054904 (2025)

- Unresolved Questions:
  - What are the dynamics governing the spatial configurations of quarks and gluons inside a proton?
  - Does this reflect manifestations of single underlying dynamical framework?

Generalized Parton Distributions

❑QCD matrix element between the p and p′

❑Non-forward limit ⟹ quark and gluon distributions

$$W^{[\Gamma]}_{\Lambda'\Lambda} = \frac{1}{2}\int \frac{d^4z}{(2\pi)^4} e^{ik\cdot z} \left\langle p', \Lambda' \middle| \bar{\psi}\left(-\frac{z}{2}\right) \Gamma \mathcal{W}\left(-\frac{z}{2}, \frac{z}{2}\middle| n\right) \psi\left(\frac{z}{2}\right) \middle| p, \Lambda \right\rangle$$

- ❑ Λ, Λ' are the initial (p) and final proton (p') helicities
- ❑ $\mathbf{\Gamma}$ is Dirac operator
- ❑ $\mathcal{W}$ is the Gauge link operator (Wilson line)

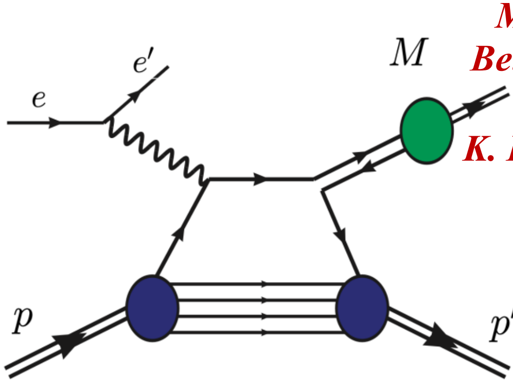

M. Diehl, Phys. Rept. 388, 41 (2003)
Belitsky and A. Radyushkin, Phys.Rept. 418, 1 (2005)
K. Kumericki, S. Liuti, and H. Moutarde, Eur. Phys. J. A52, 157 (2016)

Z. Panjsheeri, et al. arXiv: 2511.03065 (2025) Accepted in EPJC

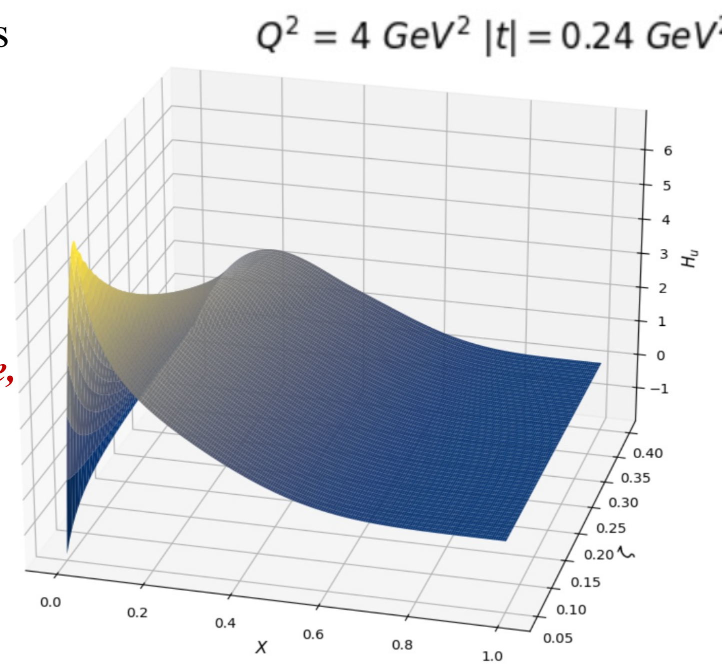

More information from GPDs

- second moment of GPDs give the total angular momentum of quarks and gluons in the proton.
- probe the energy-momentum tensor nucleon mass.
- pressure and shear forces inside hadrons → higher twist

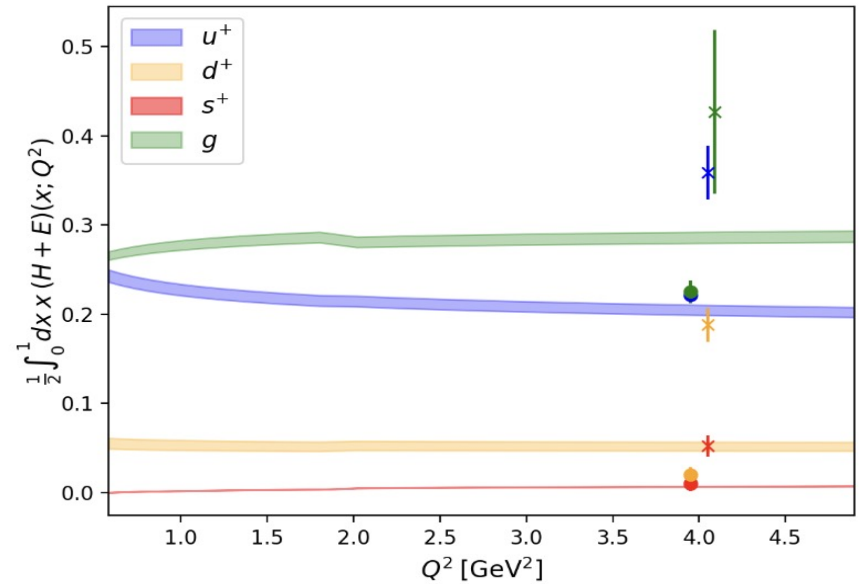

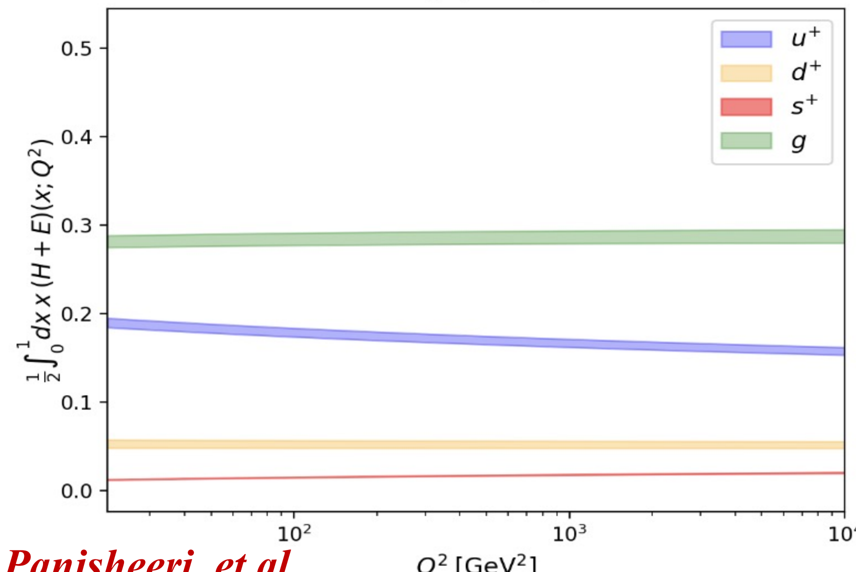

X.-D. Ji and J. Osborne, Phys. Rev. D 57, 1337 (1998)
A. Rajan, M. Engelhardt, and S. Liuti, Phys. Rev. D 98, 074022 (2018)
O. Alkasassbeh, A. Rajan, M. Engelhardt, and S. Liuti (2024)

Z. Panjsheeri, et al. arXiv: 2511.03065 (2025) Accepted in EPJC

Hackett et al. (2024, Alexandrou et al. (2020)

Disconnected picture from Lattice QCD

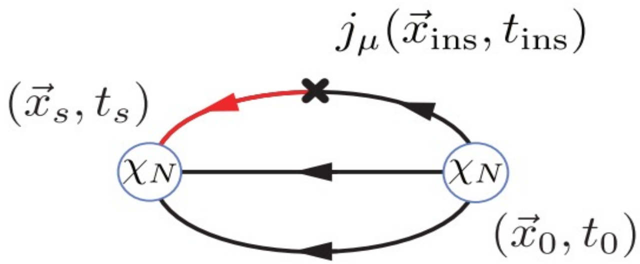

$$C(\Gamma_0, \vec{p}; t_s, t_0) = \sum_{\vec{x}_s} e^{-i(\vec{x}_s - \vec{x}_0)\cdot\vec{p}} \times \mathrm{Tr}\left[\Gamma_0 \langle \chi_N(t_s, \vec{x}_s) \bar{\chi}_N(t_0, \vec{x}_0)\rangle\right],$$

$$C_\mu(\Gamma_\nu, \vec{q}, \vec{p}\,'; t_s, t_{\rm ins}, t_0) = \sum_{\vec{x}_{\rm ins}, \vec{x}_s} e^{i(\vec{x}_{\rm ins} - \vec{x}_0)\cdot\vec{q}} e^{-i(\vec{x}_s - \vec{x}_0)\cdot\vec{p}\,'} \times \mathrm{Tr}[\Gamma_\nu \langle \chi_N(t_s, \vec{x}_s) j_\mu(t_{\rm ins}, \vec{x}_{\rm ins}) \bar{\chi}_N(t_0, \vec{x}_0)\rangle].$$

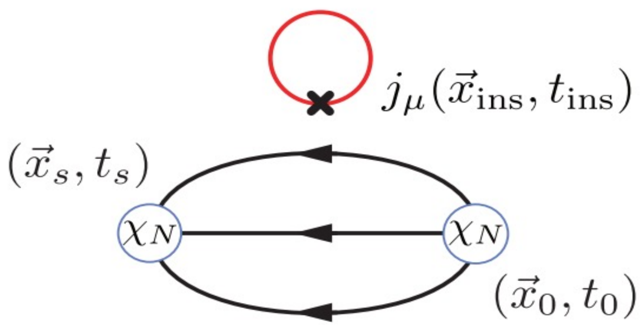

C. Alexandrou, et al.
arXiv: 2507.20910, (2025)

Disconnected:

- Has a 14 fit parameters, with three-state fits to each of the two-point functions and a two-state fit to the rotated three-point function.
- First excited-state energies between the two- and three-point functions are shared (larger statistical errors for the disconnected do not allow following the procedure of the connected analysis).

Connected:

- Multiple sink-source time separations and high statistics for both connected three- and two-point functions, a thorough analysis of excited state effect.
- Multi-state fit analysis allows different excited state energies in the two- and three-point function.
- Different fitting parameters between two- and three-point functions.
- Each fit has 31 fit parameters with no priors used in the final fit.
- First fit to the individual two-point functions, then fit the three-point functions.

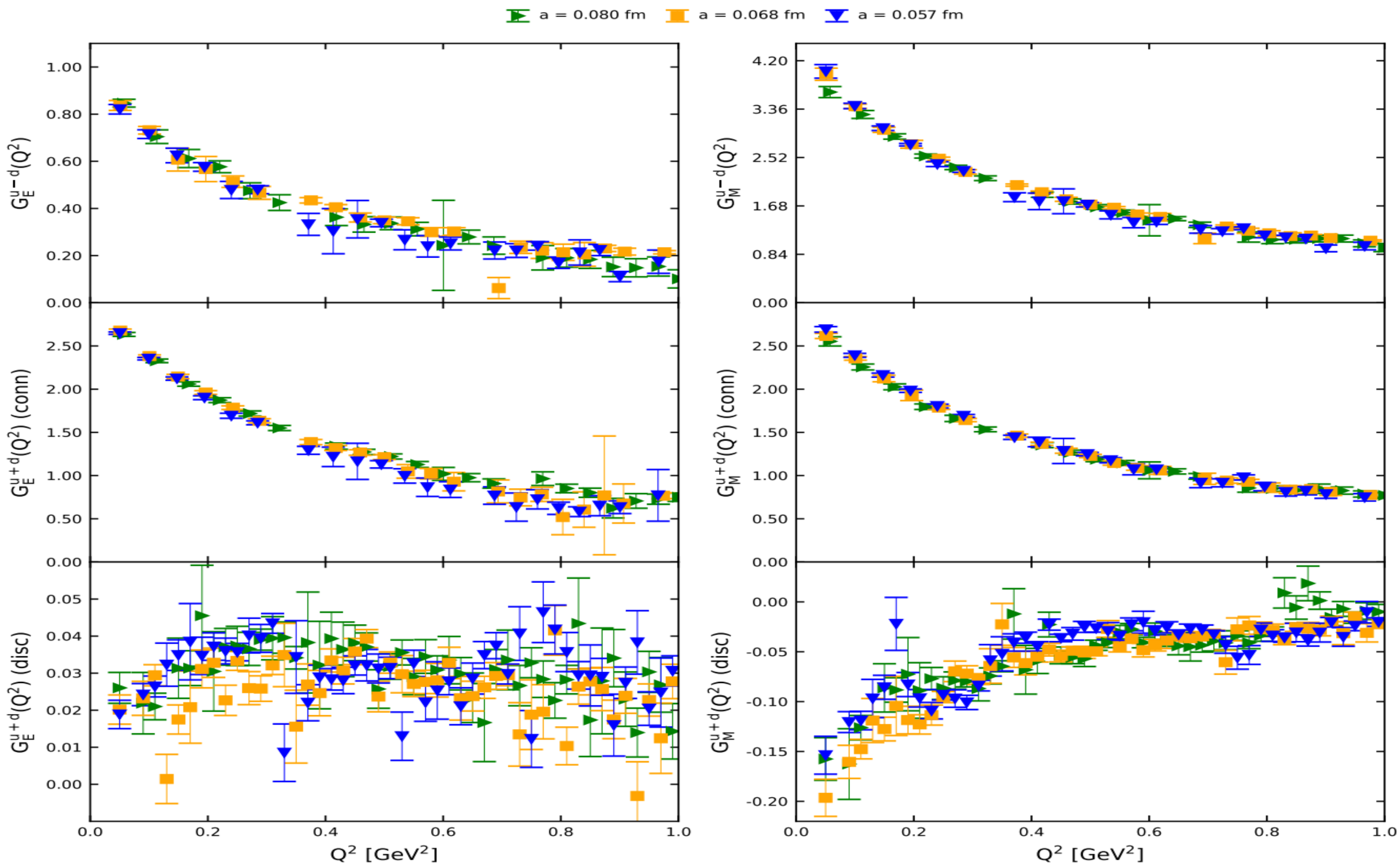

$G_E(Q^2)$ (left) and $G_M(Q^2)$ (right), connected isovector (top), connected isoscalar (middle) and disconnected isoscalar (bottom) form factors as a function of Q^2 for the three ensembles, namely cB211.72.64 (green right-pointing triangles), cC211.60.80 (orange squares), and cD211.54.96 (blue downward-pointing triangles).

C. Alexandrou, et al. arXiv: 2507.20910, (2025)

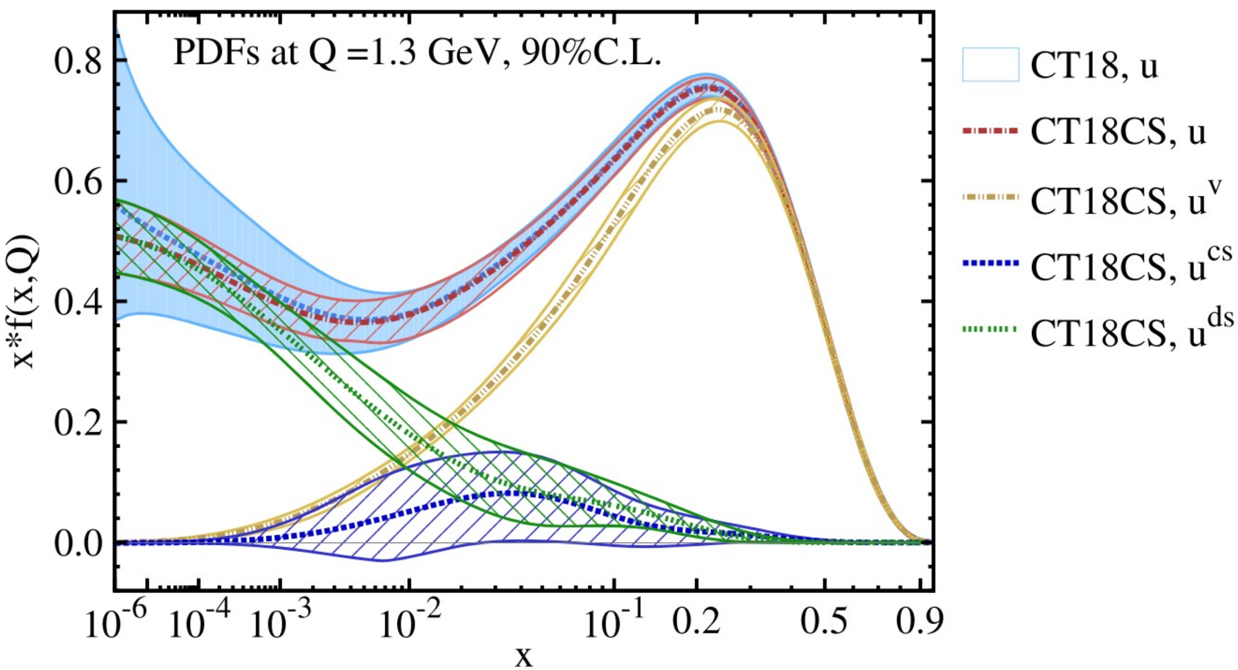

$Q_0^2 = 1.3$ GeV^2

CT18CS u and d quark distributions in the CS and DS classification

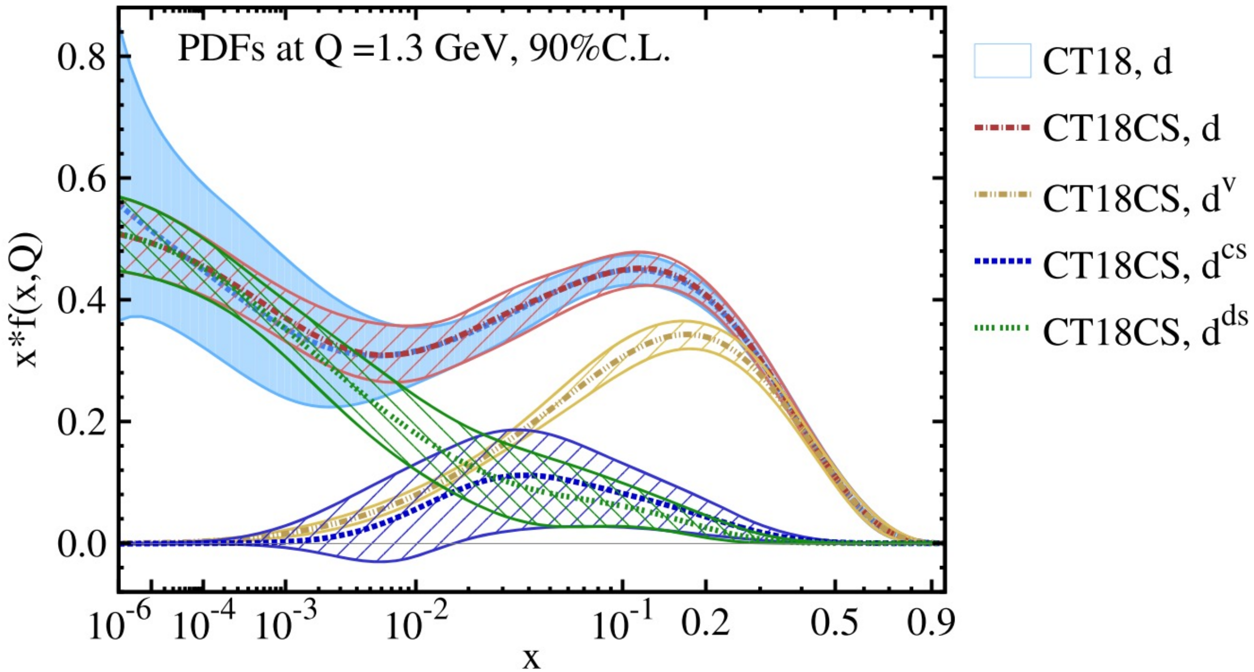

nominal CT18 NNLO

Tie-Jiun Hou, et al.
Phys. Rev. D 106, 096008 (2022)

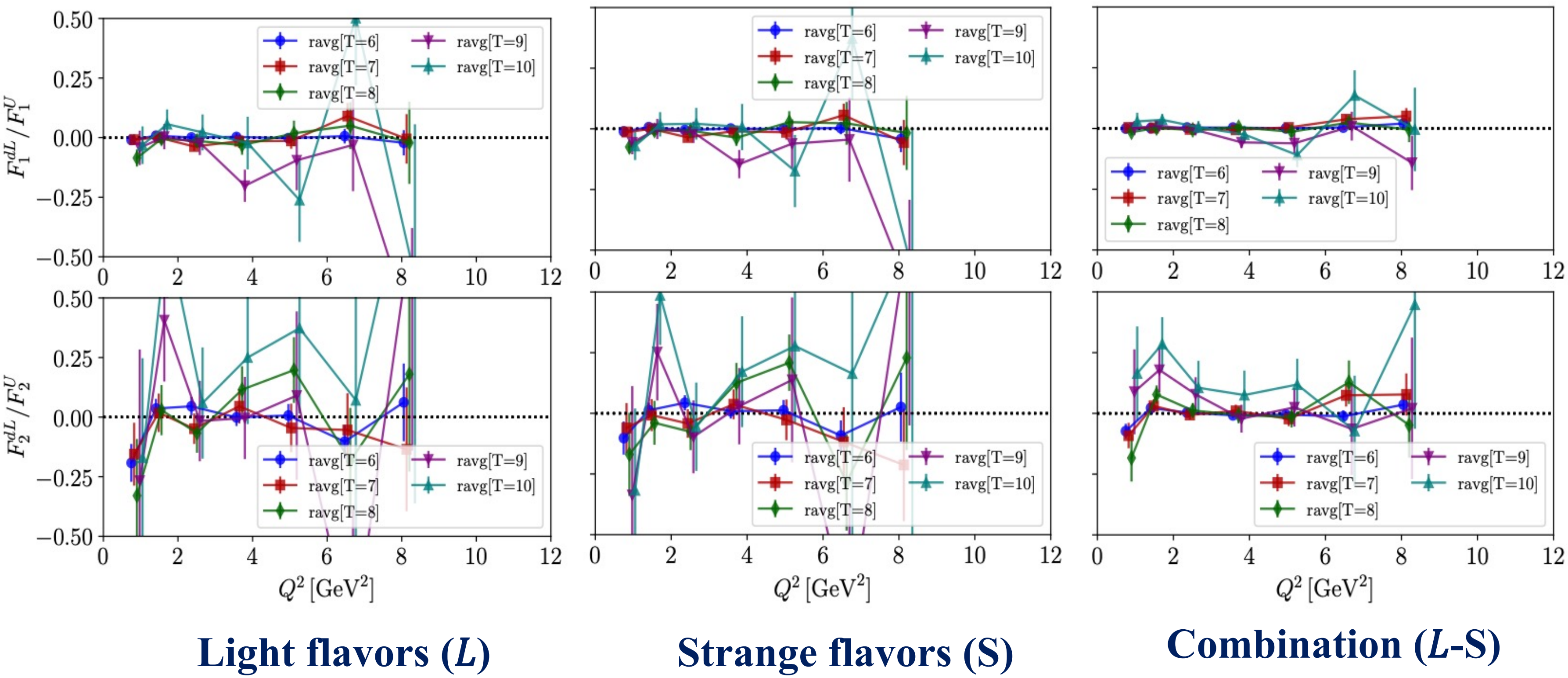

Ratio of the disconnected contributions to u quark-connected contributions to the Dirac F_1 and Pauli F_2 form factors of the proton on the D6 ($m_\pi \approx 170$ MeV) ensemble with a range of source-sink separations t_{sep}.

$$P = \frac{1}{3}[2U - D]_{\mathrm{conn}} + \frac{1}{3}[L - S]_{\mathrm{disc}}$$

$$N = \frac{1}{3}[2D - U]_{\mathrm{conn}} + \frac{1}{3}[L - S]_{\mathrm{disc}}$$

S. Syritsyn et al., PoS LATTICE2024 (2025) 340
also
Liang et al. PRD 102 (2020) 034514

UVA2 parameterization

JLAB

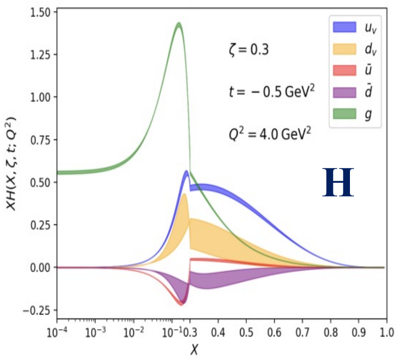

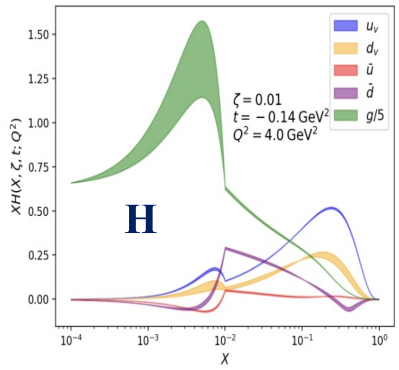

EIC

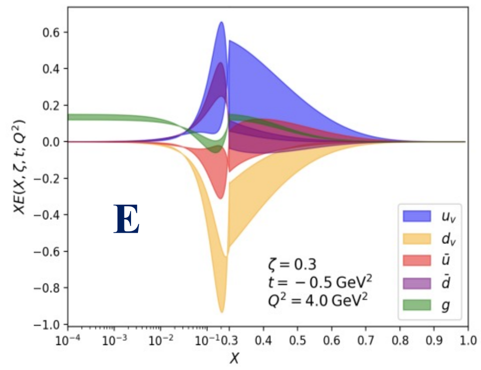

JLAB

EIC

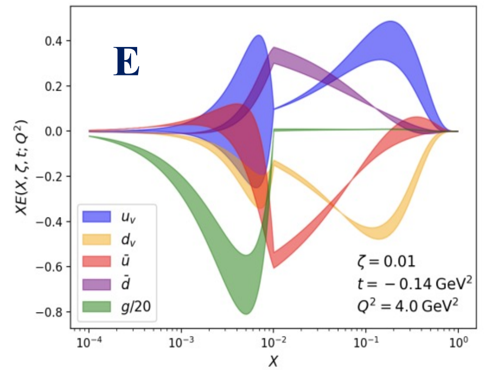

Key Features:

- **Constraint from PDFs/forward limit**: simultaneously evolve all relevant quark flavors as well as gluons, with parametrization at an initial scale of $Q^2_0 = 0.58\ \mathrm{GeV}^2$ and $\Lambda_{QCD}(N_f = 4) = 0.257$ GeV.
- **First time Analytic expressions**
- **Better Constraint on t dependence with new Lattice results**
- **QCD Evolution:** parametrization evolved at LO with initial scale of $\mu^2_0 = 0.58\ \mathrm{GeV}^2$ https://github.com/Exclaim-Collaboration/UVA2
- **Standard curve fitting procedure using MIGRAD**

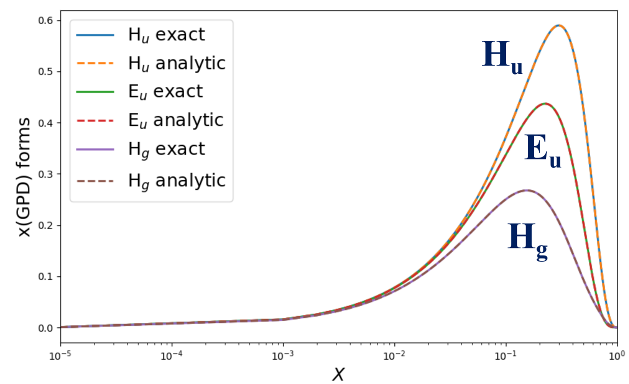

Z. Panjsheeri, et al. arXiv: 2511.03065 (2025) Accepted in EPJC

B. Kriesten, et al. Phys. Rev. D 105, 056022 (2022)

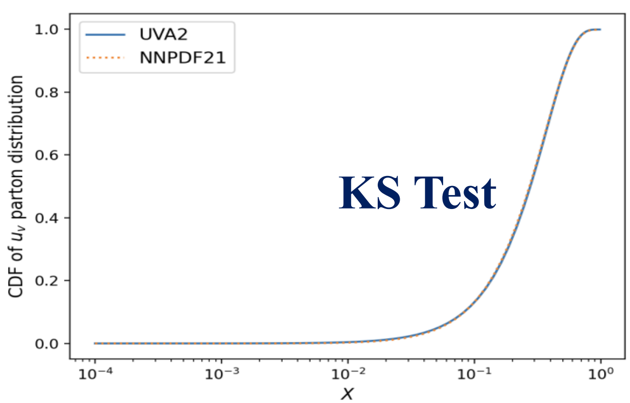

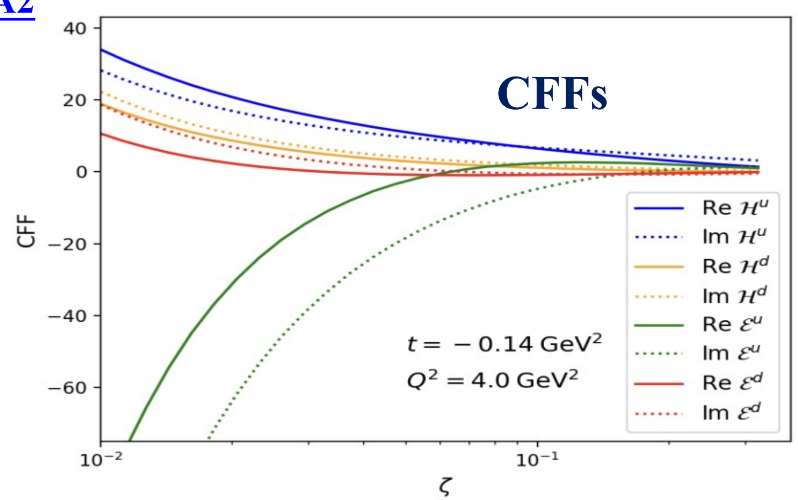

UVA2 Approach

$$H_q(x,0,0) = q(x)$$

Z. Panjsheeri, et al.
arXiv: 2511.03065 (2025)
Accepted in EPJC

$$F_1^q(t) = A_{10}^q(t) = \int_{-1}^{1} dx H_q(x,\xi,t),$$

$$F_2^q(t) = B_{10}^q(t) = \int_{-1}^{1} dx E_q(x,\xi,t)$$

Z. Panjsheeri, S. Pandey, et al.
arXiv:2512.20853 (2025)
submitted to PRL

$$M_2^{q,H}(\xi,t) = A_{20}^q(t) + (2\xi)^2 C_{20}^q(t) = \int_{-1}^{1} dx\, x\, H_q$$

$$M_2^{q,E}(\xi,t) = B_{20}^q(t) - (2\xi)^2 C_{20}^q(t) = \int_{-1}^{1} dx\, x\, E_q$$

https://github.com/Exclaim-Collaboration/UVA2

$$H_p = \sum_q e_q^2 \left(H_q + H_{\bar{q}}\right)$$

crossing symmetry

$$H_{\bar{q}}(x,\xi,t) = -H_q(-x,\xi,t)$$

$$H_q^+(x,\xi,t) = H_q(x,\xi,t) + H_{\bar{q}}(x,\xi,t)$$

$$H_q^-(x,\xi,t) = H_q(x,\xi,t) - H_{\bar{q}}(x,\xi,t)$$

Z. Panjsheeri, et al.
arXiv: 2511.03065 (2025)
Accepted in EPJC

$$H_q^-(-x) = H_q^-(x) \quad \text{symmetric}$$

$$H_q^+(-x) = -H_q^+(x) \quad \text{antisymmetric}$$

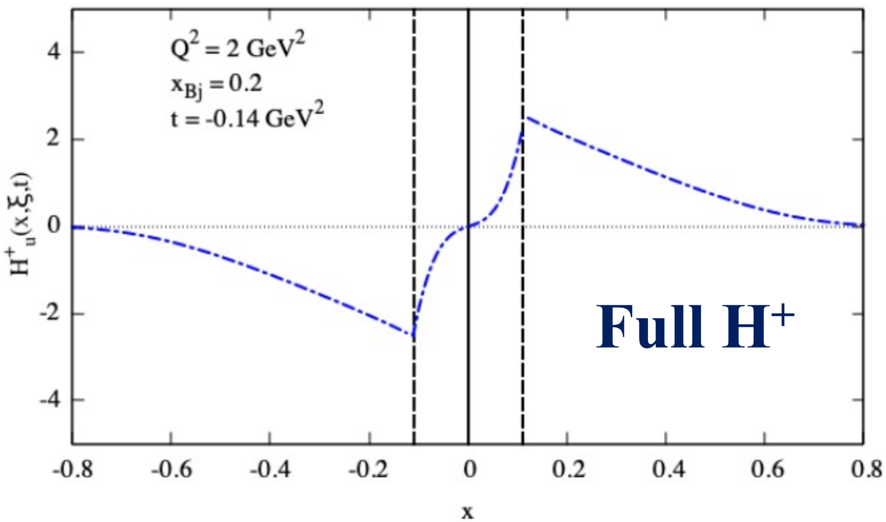

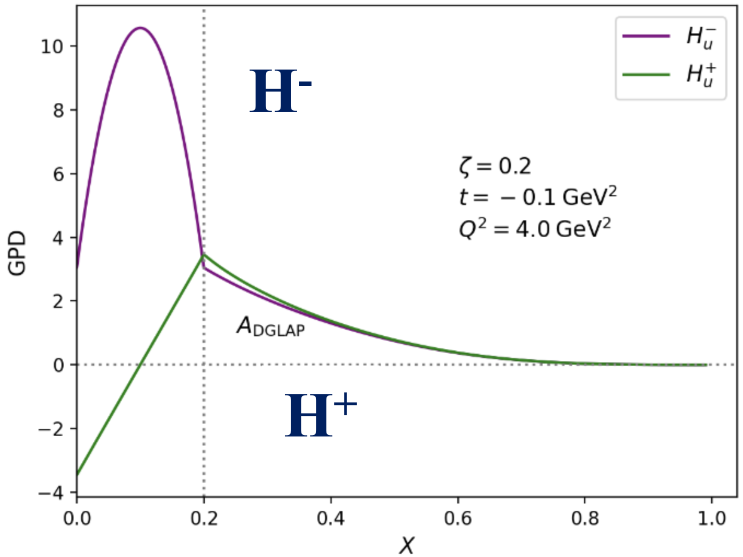

Kuti-Weisskopf ansatz

$$H_{\bar{q}} = H_{q_{sea}}$$

$$H_q^-(x) = H_{q_v}(x)$$

$$H_q^+(x) = H_{q_v}(x) + 2H_{q_{sea}}(x).$$

https://github.com/Exclaim-Collaboration/UVA2

$$F_1^q(t) \;=\; F_1^{q,C} + F_1^{q,D} = \int_{-1}^{1} dx\, H_q^C + \int_{-1}^{1} dx\, H_q^D$$

$$H_q^C \;=\; \frac{1}{2}(H_{q_v} + H_{q_{sea}}^C) = \frac{1}{2}(H_q^{-,C} + H_q^{+,C}),$$

$$H_q^D \;=\; \frac{1}{2}(H_q^{-,D} + H_q^{+,D}).$$

Z. Panjsheeri, S. Pandey, et al.
arXiv:2512.20853 (2025)
Submitted to PRL

$$M_2^{q,H}(0,t) = A_{20}^C + A_{20}^D = \int_{-1}^{1} dx\, x H_q^C + \int_{-1}^{1} dx\, x H_q^D,$$

$$H_q = H_q^C + H_q^D = \mathcal{N}_q^H x^{-\left[\alpha_q + \alpha_q'^H\, t\,(1-x)^{p_q^H}\right]} F_q^H(x,\xi,t),$$

$$H_q^{-,D} \;=\; \mathcal{N}_D^-\, x^{-(\alpha_q + \alpha_q' t)},$$
$$H_q^{+,D} \;=\; \mathcal{N}_D^+\, x^{-(\alpha_q + \alpha_q' t)}(1-x)^\beta,$$

Z. Panjsheeri, et al.
arXiv: 2511.03065 (2025)
Accepted in EPJC

Results

- Based on reggeized-spectator model, CS and DS components of GPDs is calculated.

$$H_q = H_q^C + H_q^D = \mathcal{N}_q^H x^{-\left[\alpha_q + \alpha_q'^H\, t\, (1-x)^{p_q^H}\right]} F_q^H(x, \xi, t),$$

- Recursive fitting procedure:
  - parameters determine the x shape of the distribution (fitted to PDFs, in the $(\xi, t) = 0$ limit.
  - t-dependent parameters are regulated using the flavor separated nucleon Mellin moments for n = 1, 2.
  - similar for the "+" connected contribution

- Fitting performed using the standard curve fitting procedure of MIGRAD – Minuit's principal optimization algorithm
  - efficient minimization of χ^2 through inverse Hessian matrix.

Z. Panjsheeri, et al.
arXiv: 2511.03065 (2025)
Accepted in EPJC

Z. Panjsheeri, S. Pandey, et al.
arXiv:2512.20853 (2025)
Submitted to PRL

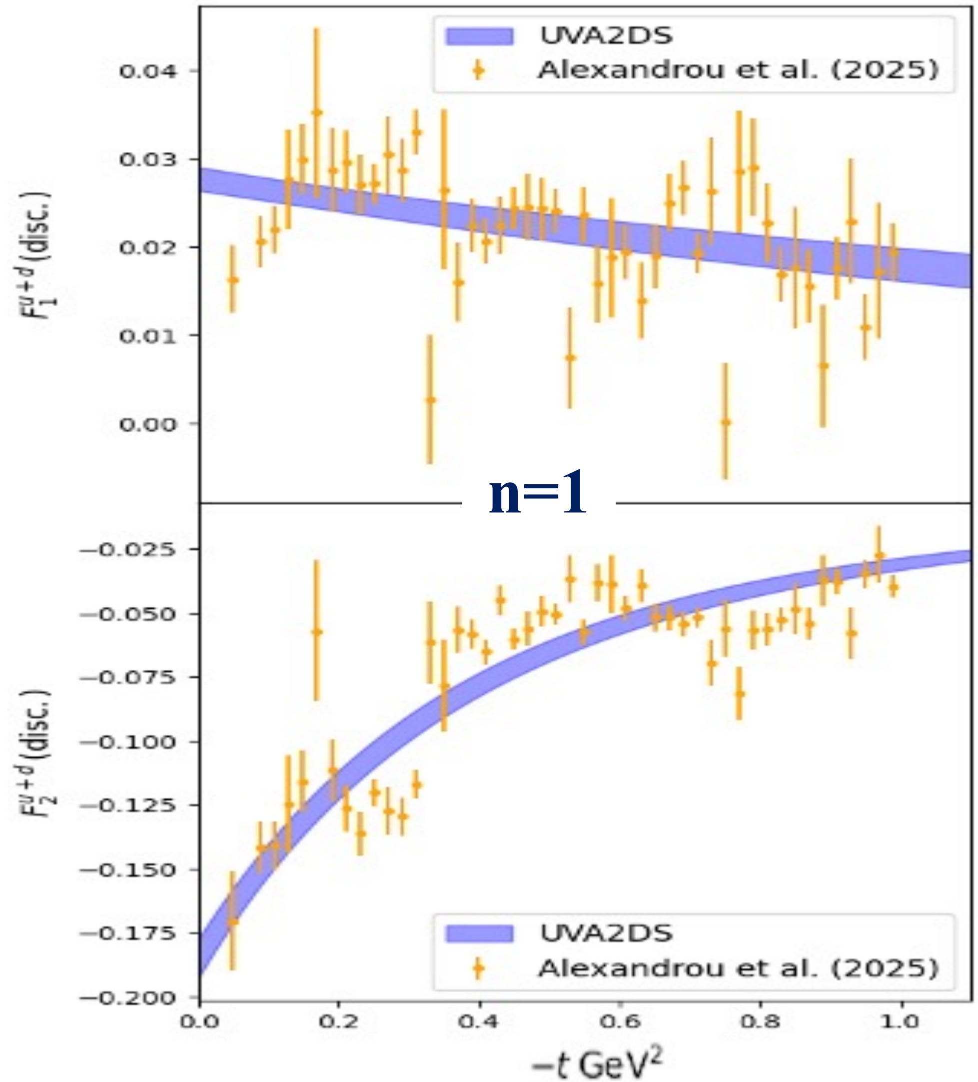

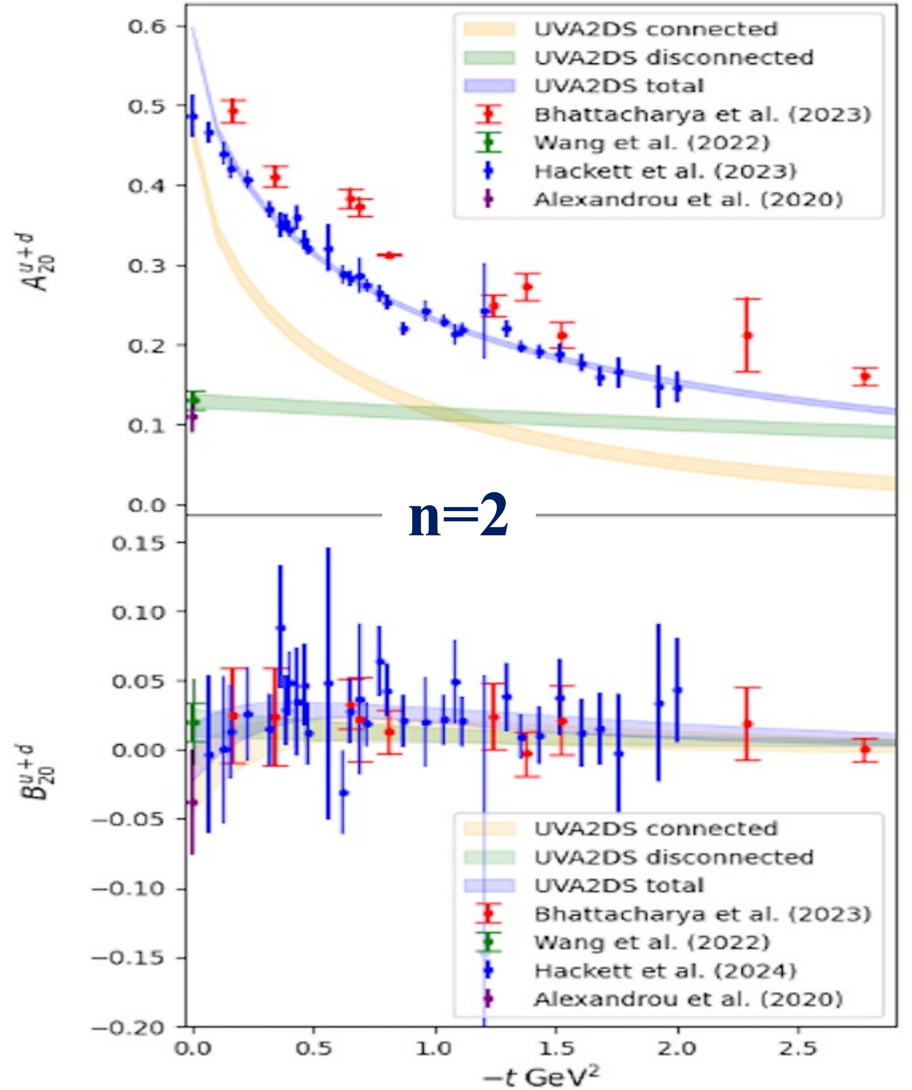

- Fit to the n = 1 (FF) DS moments compared to LQCD.
- Fit to the C+D and to the DS for n = 2 moments compared to available LQCD results.

Z. Panjsheeri, S. Pandey, et al. arXiv:2512.20853 (2025) Submitted to PRL

Hackett et al. (2024), Alexandrou et al. (2025), Wang et al. (2022), Bhattacharya et al. (2023), Alexandrou et al. (2020)

- “ – ” - symmetric components of the PDFs are obtained.

- identification of a potential disconnected contribution to the “ – ” x-distributions, in addition to the valence-quark component

- The DS component for $H^{-}_{\mathbf{u+d}}$ is small, reflecting the constraint from the small values of the corresponding calculated FFs.

- for $E^{-}_{\mathbf{u+d}}$ based on LQCD results, and lacking a constraint from the PDF in the forward limit, contribution could be large.

Z. Panjsheeri, S. Pandey, et al.
arXiv:2512.20853 (2025)
Submitted to PRL

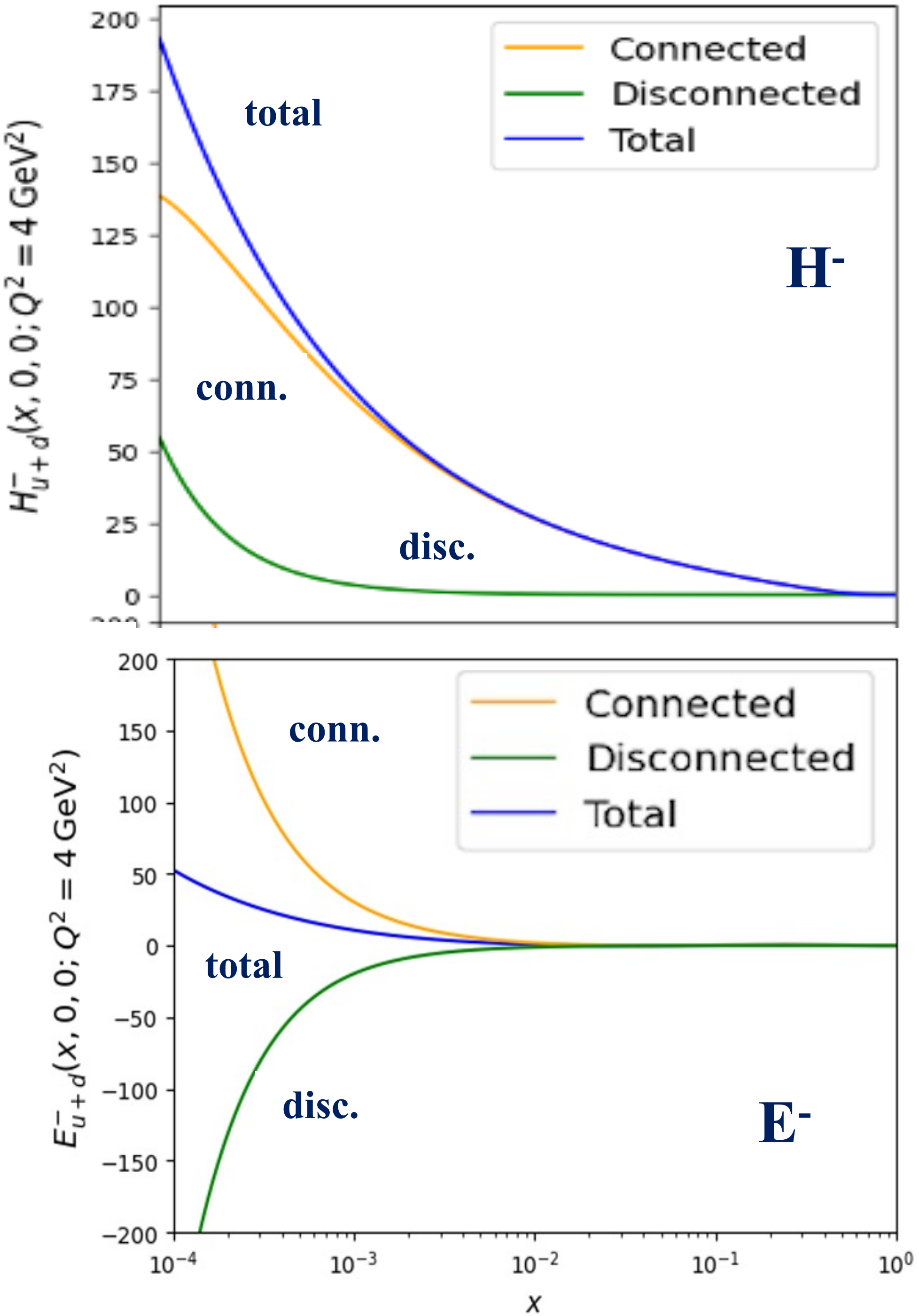

- the " + " - antisymmetric distributions of the PDFs are obtained.
- presence of a large disconnected contribution to the "+ " distributions.
- a clear dominance of the DS over the CS at low x
- underlying GPD description offers more stringent, quantitative constraints rooted in the x and t correlated structure of these quantities.

Z. Panjsheeri, S. Pandey, et al.
arXiv:2512.20853 (2025)
Submitted to PRL

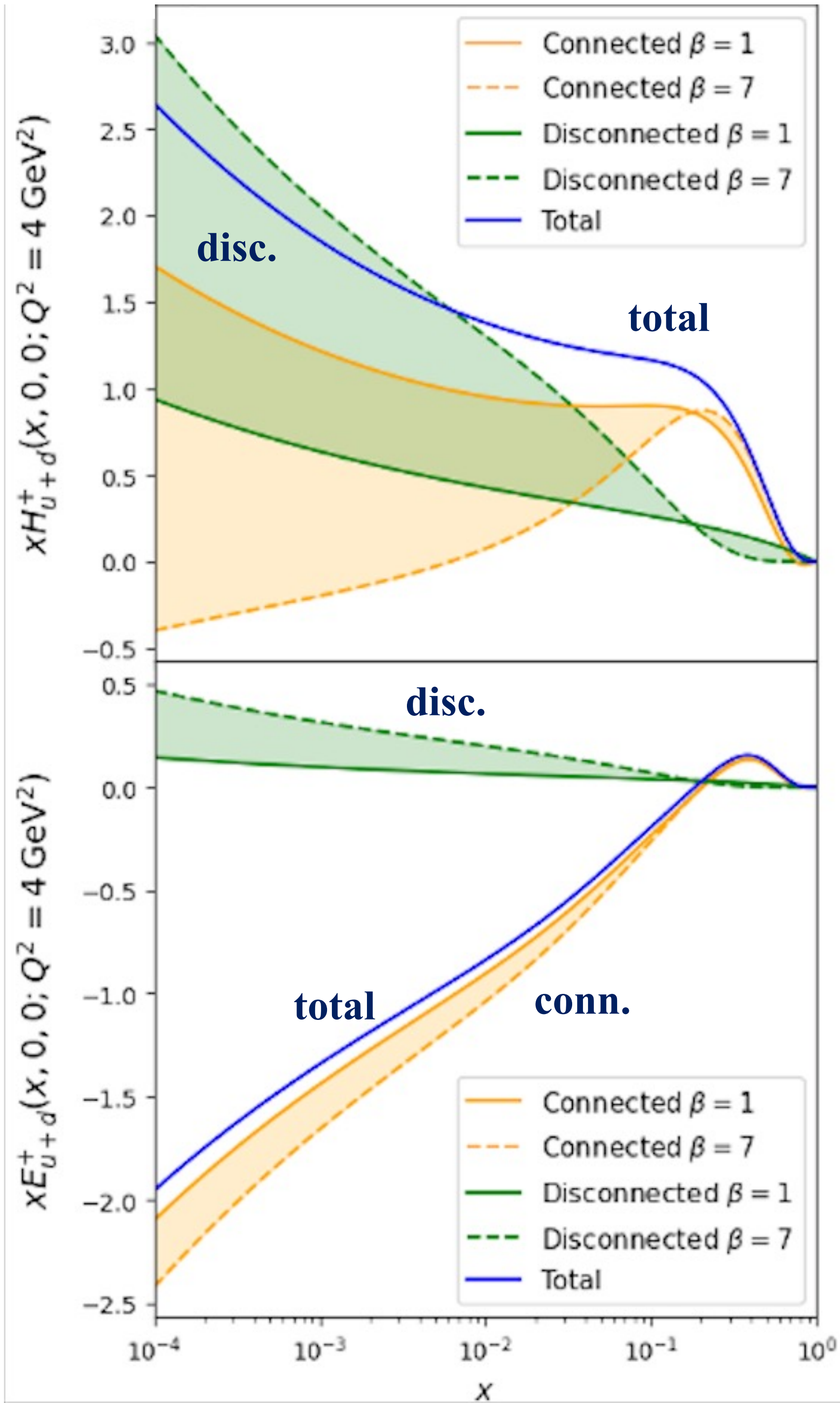

connected densities

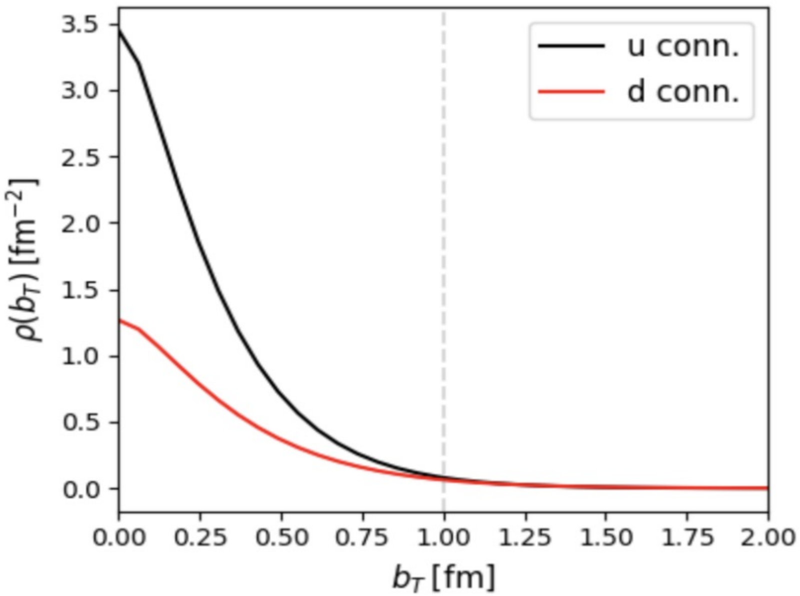

disconnected densities

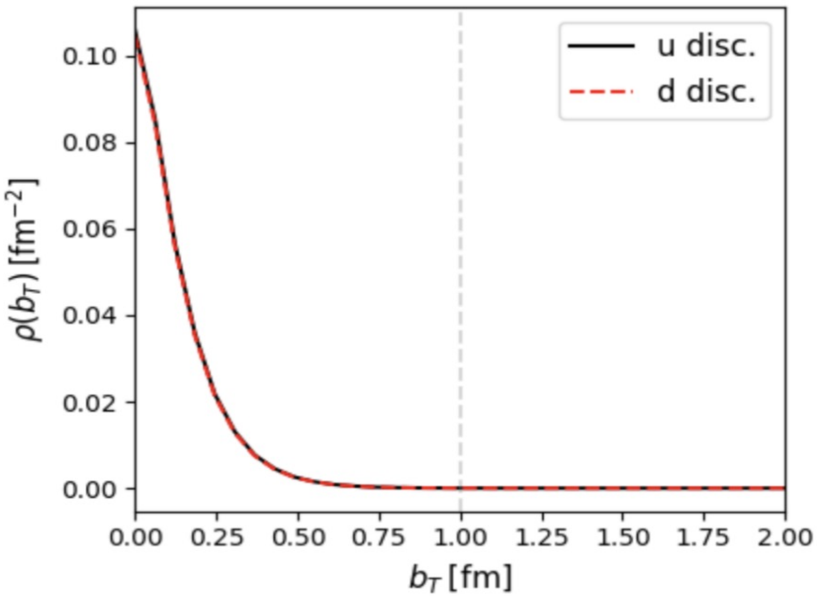

$\langle \mathbf{b}_\perp^2 \rangle^{1/2}$ [fm]	u	d
total	0.596	0.721
connected	0.601	0.734
disconnected	0.290	0.289

Mean values of the partonic radii averaged over x

- Fourier transformation of the connected and disconnected GPDs give average radii of the CS and DS per quark flavor.
- Reflecting the shape of the form factors:
  - DS is located at smaller distances than the CS, with respect to the center of momentum of the proton.

Z. Panjsheeri, S. Pandey, et al.
arXiv:2512.20853 (2025)
Submitted to PRL

Hint towards Baryon Junctions

- disconnected diagrams behavior shed light on the strangeness, $s\bar{s}$ asymmetry.

- possible connection with the baryon junction picture at low x.
  - in valence quark picture, baryon to charge transport ratio ~ 0.5-0.7 or even smaller,
  - smaller than the naive expectation of unity due to excess production of anti-strange quarks over strange quarks at mid-rapidity.
  - incorporating the baryon-junction picture via color reconnection increases the baryon to charge transport ratio ~ 0.99 ± 0.03.

- intuition of the excess of anti-strangeness observed in experiments might originate from disconnected contributions at low x.

N. Magdy, et al.
Phys. Rev. C 112, 054904 (2025)

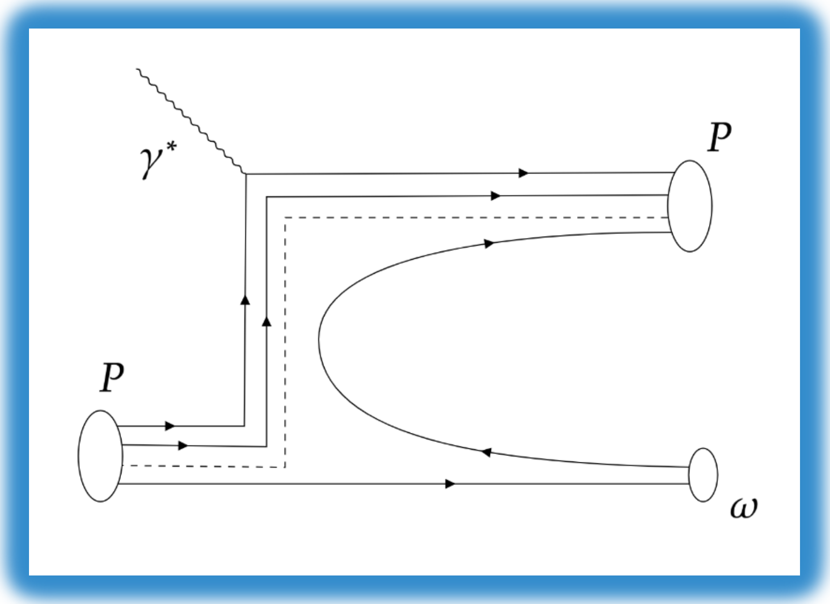

Exclusive process in which a proton is transferred to the photon fragmentation region while a ω-meson is produced in the proton fragmentation region.

D. Frenklakh, et al.
W. Li, Phys. Lett. B 853, 138680 (2024)
arXiv: 2312.15039.

Conclusions

- In summary, using the concept of GPDs, we present to our knowledge the first quantitative study of the impact of disconnected contributions to the PDFs, constrained by the values of their first (form factors) and second Mellin moments.

- We find that the effect of disconnected sea quark distributions dominates the behavior of PDFs at low values of x.

- This study of the disconnected sea represents an important step toward understanding the mechanisms responsible for the baryon–antibaryon asymmetry in QCD.

A long detailed paper soon on arXiv!!

Future Motivation

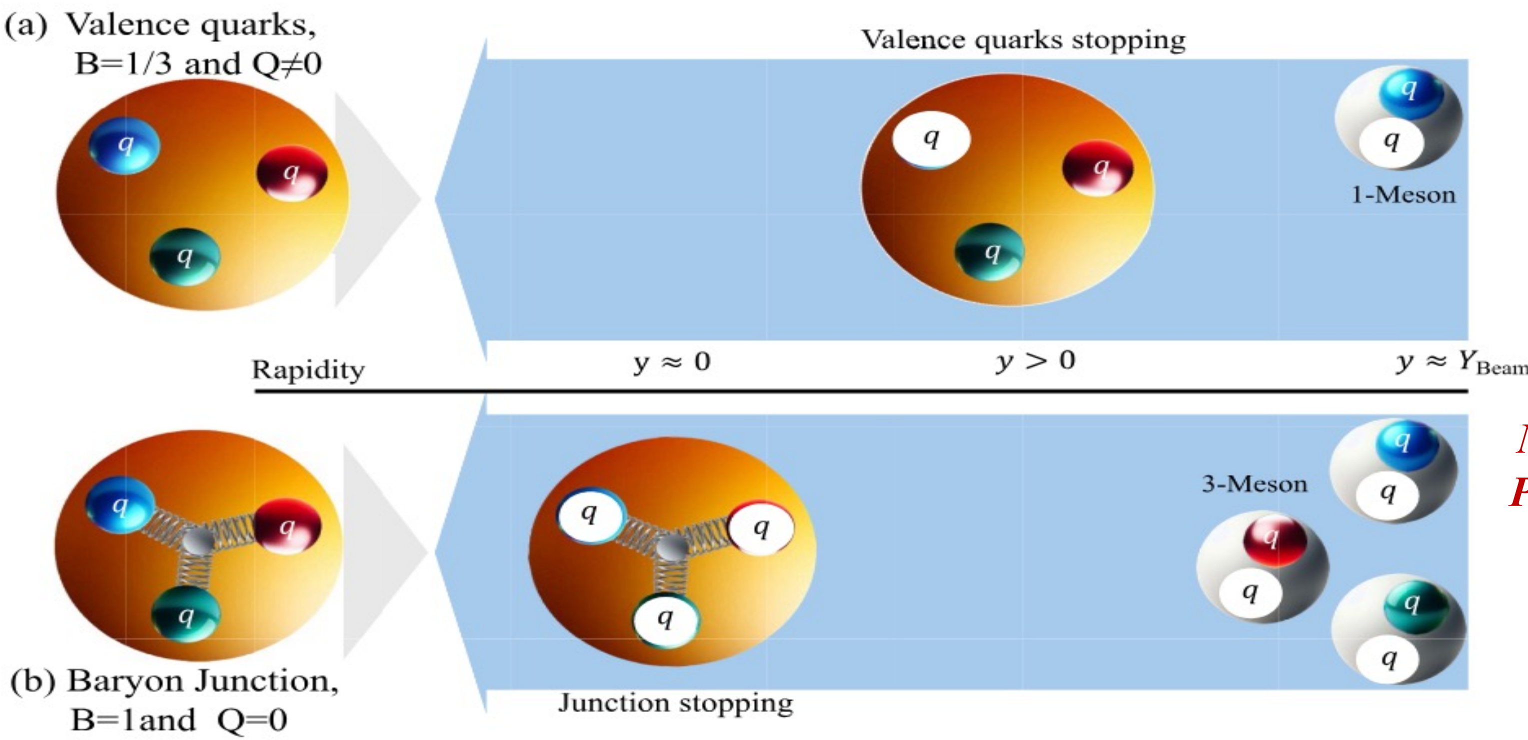

N. Magdy, et al. Phys. Rev. C 112, 054904 (2025)

$$H(x, \zeta, t) \propto exp(-\alpha \ln \sqrt{\tau}\,)\; exp(-\alpha y)$$

- ❑ Baryon Junctions for Exclusive processes
- ❑ Can we have GPD picture for Baryon Junctions
- ❑ What would the t-dependence look like for a Baryon Junction picture.
- ❑ Can we have a dynamical framework for Baryon Junctions for Exclusive processes.

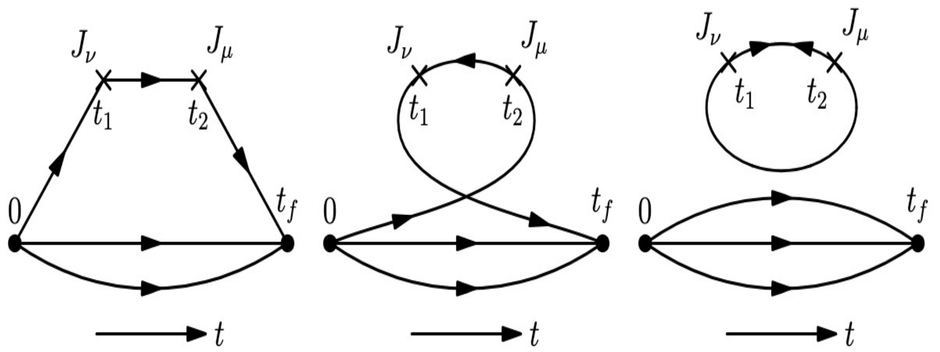

❑ QCD Evolution:

- ❑ How do the connected and disconnected distributions evolve?
- ❑ Could they be verified experimentally?

$$
\begin{aligned}
\frac{dq_i^{v+cs}}{dt} &= P_{ii}^c \otimes q_i^{v+cs} + P_{i\bar{i}}^c \otimes \bar{q}_i^{cs}; \\
\frac{d\bar{q}_i^{cs}}{dt} &= P_{\bar{i}\bar{i}}^c \otimes \bar{q}_i^{cs} + P_{\bar{i}i}^c \otimes q_i^{v+cs}; \\
\frac{dq_i^{ds}}{dt} &= \sum_k P_{ik}^{cd} \otimes q_k^{ds} + \sum_k P_{i\bar{k}}^{cd} \otimes \bar{q}_k^{ds} + \sum_k P_{ik}^{d} \otimes q_k^{v+cs} + \sum_k P_{i\bar{k}}^{d} \otimes \bar{q}_k^{cs} + P_{ig} \otimes g; \\
\frac{d\bar{q}_i^{ds}}{dt} &= \sum_k P_{\bar{i}\bar{k}}^{cd} \otimes \bar{q}_k^{ds} + \sum_k P_{\bar{i}k}^{cd} \otimes q_k^{ds} + \sum_k P_{\bar{i}k}^{d} \otimes q_k^{v+cs} + \sum_k P_{\bar{i}\bar{k}}^{d} \otimes \bar{q}_k^{cs} + P_{ig} \otimes g; \\
\frac{dg}{dt} &= \sum_k (P_{gk} \otimes (q_k^{v+cs} + q_k^{ds}) + P_{g\bar{k}} \otimes (\bar{q}_k^{cs} + \bar{q}_k^{ds})) + P_{gg} \otimes g,
\end{aligned}
$$

Keh-Fei Liu

Phys. Rev. D 96, 033001 (2017)

Acknowledge

We are grateful to Dina Alexandrou, Keh-Fei Liu, Raza Sufian, and Michael Engelhardt.

Thank you

Questions??

Back up

GPD	α_q	α'_q	p_q	$\mathcal{N}_q \times 10^{-3}$	χ^2
$H_u^{-,C+D}$ [27]	0.427	0.890(8)	0.950(27)	5930	6.7
$H_d^{-,C+D}$ [27]	0.33	0.869(33)	0.15(14)	2200	0.7
$H_u^{-,D}$	1.153	0.080(18)	–	0.629(33)	2.1
$H_d^{-,D}$	1.150	0.080(18)	–	0.629(33)	2.1
$H_u^{+,C+D}$ [27]	1.153	2.8(4)	4.9(5)	190	0.9
$H_d^{+,C+D}$ [27]	1.150	0.036(9)	−11.8(11)	1100	0.7
$H_u^{+,D}$	1.170	0.080(18)	–	99.0(91)	–
$H_d^{+,D}$	1.168	0.080(18)	–	99.0(91)	–
$E_u^{-,C+D}$ [27]	0.427	1.62(11)	1.76(9)	6870(32)	1.5
$E_d^{-,C+D}$ [27]	0.33	0.540(9)	0.10(23)	−3550(5)	0.8
$E_u^{-,D}$	1.153	0.427(23)	–	−4.62(19)	5.5
$E_d^{-,D}$	1.150	0.427(23)	–	−4.62(19)	5.5
$E_u^{+,C+D}$ [27]	0.427	0.69(7)	–	1700(16)	0.3
$E_d^{+,C+D}$ [27]	0.33	0.63(12)	–	2700(4)	0.3
$E_u^{+,D}$	1.170	0.427(33)	–	15.0(11)	–
$E_d^{+,D}$	1.168	0.427(33)	–	15.0(11)	–

Parameter values for (C+D) GPDs at an initial scale of $Q_0^2 = 0.58$ GeV^2